Version of Record: https://www.sciencedirect.com/science/article/pii/S2352938524002465
Manuscript_a9ad8a571baa27a112954d1496510ba4

# Leveraging a decade of Landsat-8 spectral records for mapping blue carbon storage in tidal salt marshes

Authors:
Daniel L Warner[1*]
Kari St. Laurent[2]
Thomas K McKenna[1]
John Callahan[3]

[1]Delaware Geological Survey, University of Delaware, Newark, DE, USA
[2]National Oceanic and Atmospheric Administration, National Ocean Service, National Centers for Coastal Ocean Science, Silver Spring, MD, USA
[3]National Oceanic and Atmospheric Administration, National Ocean Service, Center for Operational Oceanographic Products and Services, Silver Spring, MD, USA

*Corresponding author:
Daniel L Warner
257 Academy St
Newark, DE 19716
warnerdl@udel.edu

## Abstract

Tidal salt marsh ecosystems are known to accumulate and store large amounts of “blue” carbon, making them an important component of regional carbon cycle processes and a potential target for ecosystem-based carbon crediting efforts. However, blue carbon content in salt marshes can vary substantially at relatively small spatial scales. Understanding spatial variations of blue carbon storage at the landscape or local scale is important for developing carbon inventories, guiding ecological restorations, and informing habitat management strategies. We investigated the potential of spectral index records from the Landsat-8 Operational Land Imager spanning from 2014 to 2023 for mapping blue carbon storage in the soils of two tidal salt marsh systems in the Mid-Atlantic United States. The decadal mean of a non-photosynthetic vegetation index and standard deviations of a normalized difference vegetation index and a modified normalized difference water index were identified as predictors of blue carbon. These predictors were used to train a gradient boosted trees model for predicting soil organic matter content that achieved a testing set r-squared value of 0.67. We estimated that the two study marshes stored a combined 133-208 gigagrams of organic carbon in the top 30 cm of soil. We emphasize the need for better quantification of deep soil carbon in tidal salt marsh systems, which is likely quite high, and demonstrate the potential for satellite-based mapping of blue carbon within individual tidal wetland systems.



Keywords

Salt marsh, tidal wetlands, coastal, blue carbon, Landsat, remote sensing

## 1. Introduction

Coastal wetland soils are of particular importance in the global carbon cycle as they store and accumulate disproportionately large amounts of soil organic matter (SOM) and soil organic carbon (SOC) relative to their areal extent. This high carbon storage potential, in addition to many other valuable ecosystem services (e.g., shoreline protection, critical habitat, nutrient cycling), has made tidal wetlands an important target for restoration and conservation (Beaumont et al., 2014; Chmura et al., 2012). However, these soils are subjected to increasing ecological and physiochemical stressors from sea level rise, changes in storm frequency and severity, and land use conversion (DeLaune & White, 2012; Kirwan & Megonigal, 2013; Torio & Chmura, 2013). Carbon stored in coastal wetland ecosystems such as mangroves, sea grass beds, and tidal salt marshes is collectively referred to as “blue” carbon. Blue carbon is of great interest to climate change researchers, resilience planners, and policy makers, as the aforementioned stressors may reduce carbon accumulation and possibly lead to enhanced carbon loss due to erosion and mobilization, vegetation stress, and alterations to sediment supply (Andersen et al., 2011; Chmura et al., 2003; McLeod et al., 2011; Mueller et al., 2019; Steinmuller & Chambers, 2019; Theuerkauf et al., 2015). Conversely, the preservation and restoration of blue carbon ecosystems may enhance estuarine carbon storage, providing both ecological and potential economic benefits. Indeed, the mapping, preservation, and restoration of blue carbon ecosystems has been highlighted as a priority in the United States Ocean Climate Action Plan (Ocean Policy Committee, 2023). Though its importance is clear, there are still many unknowns surrounding blue carbon processes, especially in the face of climate change. Improving our understanding of spatial patterns of SOM and SOC in tidal salt marshes will help identify conservation priorities at local scales and constrain carbon stock estimates at regional-to-global scales.

The issue of scale is important when considering spatial patterns of blue carbon storage. In a national scale analysis, Holmquist et al. (2018) found that soil organic matter content in tidal wetlands followed a roughly normal distribution, with variations across marsh systems being only minimally influenced by local climate, salinity, and vegetation characteristics. These findings were supported by a second national scale analysis (Uhran et al., 2021), underscoring the diminished influence of local scale variations on large scale SOM and SOC storage estimates. However, it is known that SOM and SOC storage can vary substantially within a salt marsh system at the landscape and plot scale (Fettrow et al., 2023; St. Laurent et al., 2020). While using a national average may be adequate for continental or global carbon cycle modeling, accounting for spatial variations within a marsh system may help guide ecological restorations or conservation strategies that operate on a much more localized scale. Notably, recent studies have highlighted the potential of carbon crediting systems for offsetting the costs of localized blue carbon ecosystem restorations (Oreska et al., 2020). Despite its potential role in carbon markets, methods for accurately quantifying blue carbon storage at the landscape scale are still an area of developing research. Identifying marsh features with high or low SOM storage potential may help prioritize marsh tracts that would benefit most from targeted conservation strategies or restoration practices to enhance climate resiliency.

*In situ* sampling for blue carbon mapping across tidal salt marsh landscapes is challenging. Their soft soil, dense vegetation, and environmental protection status prevent the use of heavy sampling equipment and make them difficult to traverse on foot. Sampling from boats limits soil collection to near-channel areas of the marsh, neglecting the marsh interior, while sampling from the marsh fringe can make site access difficult. As salt marshes are critical habitats for imperiled or endangered species, federal and local protections often necessitate site access permits from federal and state governments and conservation agencies. These understandable challenges make large sampling campaigns in salt marshes difficult and time consuming, making traditional soil mapping techniques (e.g., interpolations and manual unit delineations) challenging and potentially less accurate (Holmquist et al., 2018). To overcome these logistical challenges researchers have begun to employ techniques in the field of digital soil mapping that utilize increasingly abundant and data-rich products from aerial and satellite remote sensing platforms (Araya-Lopez et al., 2023; McBratney et al., 2003; Sharma et al., 2022). Studies seek to map soil properties based on statistical relationships between *in situ* soil sample data and remote sensing covariates over broad spatial scales. While remote sensing platforms cannot directly observe SOM and SOC, they can observe surficial environmental characteristics like vegetation phenological stages, soil saturation, weather patterns, surface temperature, and terrain characteristics. These variables can relate to spatiotemporal patterns of soil characteristics, making remote sensing an increasingly important tool for soil science in tidal salt marshes and many other ecosystem types.

The use of remote sensing in blue carbon mapping is an area of active research. Wardrup (2021) mapped salt marsh SOC across the northeastern United States using a regional scale model trained on observations from a variety of sources with a mixture of static elevation data and vegetation indices from high spatial resolution aerial imagery (3 m; U.S. Department of Agriculture's National Agricultural Imagery Program). These maps revealed substantial small scale spatial heterogeneity in SOC stocks, but also highlighted the substantial uncertainty of model predictions and inconsistencies of SOC stock estimates across different studies. Zhang et al. (2019) used aerial hyperspectral imagery (visible and near-infrared ranging 400-980 nm) to map various salt marsh SOM content using object-based image segmentation and machine learning-based classifications. Their approach showed promise for mapping local scale variations in SOM, but required costly hyperspectral data collections that are not available for most salt marshes. Predictions made with data simulated to reflect more accessible commercial satellite data (i.e., Worldview-2 and Quickbird) indicated reduced performance. Similarly, Villoslada et al. (2022) found that aboveground biomass maps generated from multispectral drone imagery (4-band ranging 530-810 nm) were stronger predictors of organic carbon concentrations in tidal wetland soils than flooding frequency estimated from publicly-available satellite radar imagery (Sentinel-1). The authors also found that different predictors were better suited for different systems, indicating that there is no single data source that works best for blue carbon mapping across all systems. Thus, developing landscape scale maps of blue carbon storage is possible, but there is a continuing need for exploration of statistical methods and publicly available, widespread remote sensing predictors to achieve this.

Soils are products of long-term environmental processes. In the case of tidal salt marshes, soil evolution is dependent on long-term cycles of tidal inundation, vegetation productivity and structure, salinity regime, decomposition rates, and sediment deposition (Fagherazzi et al., 2012; Witte & Giani, 2017). Monitoring these processes *in situ* across an entire marsh system over multiyear timescales is a massive undertaking, but some remote sensing missions, like Landsat-8 and its Operational Land Imager (OLI), now provide multispectral information spanning over a decade. Numerous spectral indices have been developed that reflect vegetation health, biomass, soil moisture and inundation status, and other relevant ecological characteristics (Montero et al., 2023). In this study, we investigated the potential of statistics extracted from decadal spectral indices derived from the Landsat-8 OLI for modeling and mapping spatial patterns of organic matter storage in tidal salt marsh soils. In this paper, we use the term “decadal” to indicate the span of Landsat-8 images used to generate summary statistics (e.g., mean and standard deviation) of various spectral indices. Specifically, we asked: 1. Which statistics of established spectral indices show correlations with SOM storage? 2. What is the degree of sub-pixel heterogeneity of SOM storage (i.e., how much does SOM density vary within a Landsat-8 OLI pixel footprint)? 3. How do predictions of whole marsh SOM and SOC storage compare to those derived from other approaches in the literature? The purpose of this work was to develop a modeling approach that supports ongoing blue carbon mapping and quantification efforts using the wealth of publicly available satellite data that has been collected. We addressed these questions in two tidal salt marsh systems in Delaware Bay, Delaware, USA, and provide insights that may help guide future blue carbon mapping and accounting efforts in other tidal salt marshes (Fig 1).

## 2. Methods

### 2.1 Study areas

This study focused on the Delaware tidal salt marshes surrounding Blackbird Creek and St. Jones River, both of which feature areas managed by the Delaware National Estuarine Research Reserve. These study marshes were selected for their numerous site access points and history of use in environmental research. Both study marshes occupy watersheds with extensive land use modification, including manmade impoundments. The Blackbird Creek watershed is a blend of row crop agriculture (39%), wetlands (25%), forest (22%), and low intensity urban development (~10%). The St. Jones River watershed features extensive urban and suburban development (25%) surrounding the city of Dover including a large reservoir and a sand mining operation. This watershed also features extensive agriculture (48%) with some forests (10%) and wetlands (14%) (DNERR 1999). Wetland footprints were delineated based on vegetation maps that were subsampled to include only polyhaline or mesohaline emergent vegetation communities and mudflats (i.e., woody forests and freshwater wetlands were removed) delineated by Coxe (2010). The footprints of each wetland network were 1372 and 1402 ha, respectively. Dominant vegetation types include *Spartina alterniflora*, *Spartina patens*, and the invasive *Phragmites australis*, which collectively cover almost the entirety of each study marsh (Fig S1; Fig S2). These systems are affected by upstream agriculture and suburban development, which may alter sediment supply and chemistry. They are also experiencing a relatively high (and accelerating) rate of sea level rise (up to 5.94 mm $yr^{-1}$; Callahan et al. 2017) due to regional land subsidence from glacial isostatic adjustment, changing ocean currents, and increases in the global mean sea level from thermal expansion and melting ice sheets (Sweet et al., 2022).

Sampling points were identified based on site accessibility and supplemented an existing soil sample dataset (St. Laurent et al., 2020). The existing dataset consisted of samples primarily collected by boat near major wetland channels, while the new sampling points captured sites along the outer wetland and in the upper and interior areas (Fig 1). The combined sample set reflects an array of different sedimentary environments with respect to marsh platform elevation, distances from channels and fringes, microtopography, inundation regime, and vegetation communities.

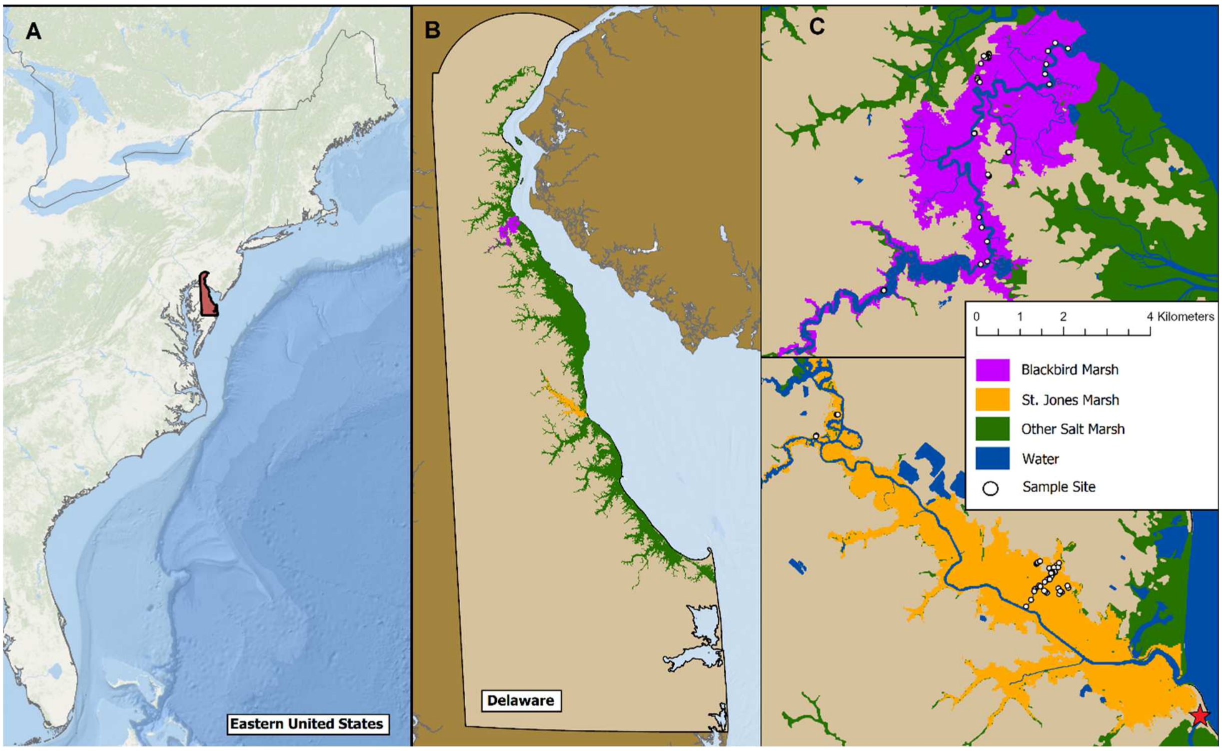


**Figure 1. Map of study sites in the context of the eastern United States. The location of the USGS Murderkill River tide gauge can be seen in the lower right of panel C as the red star near the outlet of St. Jones River.**

## 2.2 Soil sample collection and analysis

Soil samples for this study were collected using a gouge auger inserted 1 meter (if possible) into the sediment along pre-planned transects during the 2020 growing season (May – September). Samples were collected in triplicate within an approximately 1-meter radius at each sampling location and the top 30 cm segment of each core was reserved for further analysis. If sufficiently intact, additional segments were collected from 40 to 60 and 70 to 90 cm. Each sampling location was occupied with a GPS unit until roughly 1-meter horizontal accuracy was achieved. Triplicate core segments were placed in a plastic sample bag in the field and placed on ice before transporting to the laboratory. Segments were then air dried at room temperature in a constantly flowing exhaust hood until reaching a stable mass. This mass was normalized to the known volume of each segment to calculate the bulk density (BD). Triplicate segments were then homogenized into one sample, ground, and sieved to 2 mm to remove large stones and pieces of undecomposed plant material.

Samples were analyzed for organic matter content via loss on ignition (LOI) following a similar method to Heiri et al. (2001). Approximately 10 g of homogenized sample was placed into foil containers with small perforations to allow gas to escape. Samples were combusted at 550 °C for 6 hours in a vented furnace and reweighed after cooling. This amount of time was found to yield a stable final mass (several preliminary test samples were combusted for 4, 6, and 8 hours). LOI was calculated as a percentage of mass loss before and after combustion. SOM density per unit volume was then calculated as the LOI multiplied by the sample BD (g $cm^{-3}$). For surface samples, organic matter density was then converted to a mass per unit area (kg $m^{-2}$) by multiplying by sample depth of 30 cm, from here on referred to as $SOM_{30}$. Subsamples of combusted residue were retained for elemental (C and N) analysis to estimate the inorganic fraction of carbon in the soils.

Samples from St. Laurent et al. (2020) were collected in the top 30 cm during the growing seasons of 2017 and 2019 but were sectioned differently than the previously described method. Most samples were sectioned at 0-15 and 15-30 cm while some were sectioned at 0-7.6 and 22.8-30.4 cm. Each sample was similarly analyzed for BD, LOI, and percent C content. To account for differences in the core sectioning, soil property values for the upper 30 cm were calculated as a weighted sum based on relative segment lengths and their corresponding soil properties. This allowed for comparisons across both datasets, though we note that this may be a cause of minor uncertainty in $SOM_{30}$ values for samples sectioned at 0-7.6 and 22.8-30.4 cm.

All samples were analyzed for elemental C and N content using an Elementar Vario EL Cube at the University of Delaware Advanced Materials Characterization Laboratory (Newark, DE, USA). Dried soils were ground to a fine powder, and between 40 and 100 mg of sample was encapsulated in tin foil capsules, with final weights recorded to four decimal places. Lower weights were used for high LOI samples to avoid potential detector saturation. Duplicate capsules were used to ensure consistency in elemental composition within samples. All samples were analyzed for C and N content, and a majority of post-LOI residues from surficial samples were analyzed to estimate inorganic fractions of C. Using this information, we estimated the percentage of organic C (OC) contained in total organic matter. This percentage was later used for whole marsh estimates of SOC content.

## 2.3 Landsat images and derived spectral indices

This study employed spectral imagery from the Landsat-8 OLI for generating spatial predictors of marsh $SOM_{30}$ density. This platform passes the study area at 15:40 GMT with a 16-day revisit cycle and provides imagery in multiple spectral bands. This study employed blue (450-510 nm), green (530-590 nm), red (640-670 nm), near-infrared (NIR; 850-880 nm), and shortwave infrared (SWIR1; 1570-1650 nm and SWIR2; 2110-2290 nm) bands. Tier 1 scenes from 2014 to 2023 with less than 30% cloud cover were downloaded using the US Geological Survey Earth Explorer “landsatxplore” Python API, yielding a total of 75 scenes within a roughly 3- to 4-year time interval of soil sample collections. This collection of scenes captured both seasonal variations in plant phenology and the broad range of tidal conditions present during the period of record. Scenes were nearly evenly distributed across winter (DJF; n = 18), spring (MAM; n = 16), summer (JJA; n = 20), and fall (SON; n = 21). Tidal records from the mouth of the nearby Murderkill River (USGS gauge 01484085) were compared to tidal conditions at the time of Landsat-8 flyover. Although Landsat-8 collections did not replicate the frequency of the higher end of the tidal cycle, they did capture the full range of tidal stages at this gage (Fig 2). Thus, it should be noted that the Landsat-8 imagery collection utilized in this study may skew slightly towards lower tidal conditions. It should also be noted that tidal schedules and amplitudes at the reference gage are not necessarily representative of those within the study marshes, as tides are dampened and require time to propagate through the marsh channel networks.

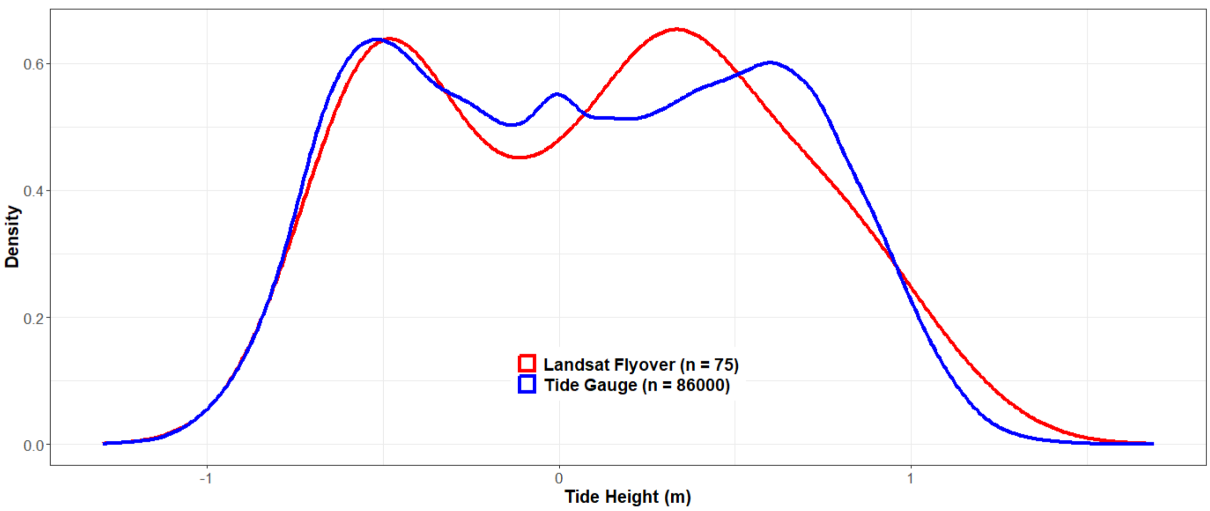

**Figure 2. Kernel density estimates were used to visually compare distributions of hourly tide gauge levels (blue) from the nearby Murderkill River from 2014 to 2023 (USGS 01484085) to those at the time of Landsat-8 image collections (red) during this same study period.**

Pixels flagged for clouds and cloud shadows in the Landsat-8 Level-1 Quality Assessment (QA) band were removed to include only pixels corresponding to clear land surface and open water. These filtered scenes were stacked into a data cube, and a variety of normalized difference spectral indices (NDIs) were calculated as potential predictors for $SOM_{30}$. These follow a generalized formula of:

$$\mathrm{NDI}_{a,b} = (\mathrm{Band}_a - \mathrm{Band}_b)/(\mathrm{Band}_a + \mathrm{Band}_b) \qquad [1]$$

Where $NDI_{a,b}$ is the normalized difference index and Bands a and b are specific Landsat-8 spectral bands. A full list and description of indices considered in this study are available in Table 1. This list includes indices developed for mapping vegetation phenology and productivity, litter biomass, and surface water features.

Decadal statistics of mean (.mean), standard deviation (.sd), range (.rng), and coefficient of variation (.cv) of each spectral index were calculated for each pixel over the study period (2014-2023). These statistics were calculated at the same 30 by 30 m pixel resolution of the original Landsat-8 images, though we note that there can be some blurring from image to image that may introduce small errors into single pixel time series. Once derived, spectral index statistics were extracted for each pixel corresponding to a soil core sampling location. In 18 cases, multiple core samples corresponded to one single pixel, and these were used in later assessments of sub-pixel $SOM_{30}$ heterogeneity. It should be noted that no significant construction or land modifications occurred in the two marshes during the time interval considered in this study.

**Table 1. Overview of spectral indices considered as predictors of $SOM_{30}$ in this study.**

| Name | Formula | Description | Citation |
|---|---|---|---|
| Normalized Difference Vegetation Index (NDVI) | $NDI_{NIR,Red}$ | A commonly used index for assessing vegetation greenness and phenological stage | Rouse et al. 1974 |
| Normalized Difference Water Index (NDWI) | $NDI_{Green,NIR}$ | Developed for delineating surface water features | McFeeters 1996 |
| Nonphotosynthetic Vegetation Index-1 (NPV1) | $NDI_{Blue,Green}$ | Developed for differentiating vegetation types, living and dead biomass*. | Beana et al. 2017; Byrd et al. 2018 |
| Nonphotosynthetic Vegetation Index-2 (NPV2) | $NDI_{SWIR1,SWIR2}$ | Developed for estimating crop residues in fields*. | Daughtry et al. 2006 |
| Modified Normalized Difference Water Index-2 (MNDWI2) | $NDI_{Green,SWIR2}$ | Developed for identifying fine drainage canals and hydrologic features. This index is also affected by soil moisture content. | Reddy et al. 2018 |

*NPV is often modeled with indices derived from fine differences in shortwave infrared (SWIR) spectral region, however Landsat-8 OLI lacks sufficient band resolution in this region to generate the most commonly accepted spectral NPV indices (Dennison et al., 2023). For this reason, we assessed the potential performance of two less-common indices that align with Landsat-8 OLI bands.

## 2.4 Modeling

The first step in modeling $SOM_{30}$ based on spectral characteristics was to extract all spectral index statistics for pixels containing a sample site to their corresponding $SOM_{30}$ value (or values, in the cases of pixels containing multiple sampling sites). $SOM_{30}$ and corresponding spectral index statistics were split into training (80%) and testing (20%) sets. The next step was to pare down the list of potential predictors (e.g., NDVI.mean or NPV2.sd) to remove poorly correlated and/or redundant predictors. This was done by iteratively excluding each potential predictor from a series of multiple linear regressions with $SOM_{30}$ and calculating the variance inflation factors and correlation coefficients for each iteration. This ultimately yielded a final set of strong predictors all with a variance inflation factor of less than 1.5, indicating very little multicollinearity amongst predictors. Weak or redundant predictors were discarded.

These final predictors were used to generate a multiple linear regression and a gradient boosted regression trees model for predicting $SOM_{30}$ based on the spectral characteristics of pixels corresponding to sampling locations. Gradient boosted tree is a regression tree-based algorithm that builds a series of weak learning trees using residuals of previous trees over a series of training iterations. This algorithm was chosen due to its relative ease of training, ability incorporate non-linear variable relationships, and established performance in blue carbon mapping (Pham et al., 2023). In the case of the gradient boosted trees regression, model hyperparameters were tuned via 5-fold cross validation using the "caret" (Kuhn 2008) and "xgboost" (Chen et al. 2024) packages in R statistical software version 4.3.3 (R Core Team 2024). After tuning, the final models were fit and extrapolated to our testing set data to generate performance evaluation metrics of mean absolute error (MAE), root mean square error (RMSE), and the coefficient of determination ($R^2$).

## 3. Results

### 3.1 Soil bulk density, organic matter density, and carbon content

Soil bulk density ranged from 0.23 to 1.5 g $cm^{-3}$ in the upper 30 cm with a mean of 0.65 g $cm^{-3}$. Deeper soil layers had significantly higher bulk density (t-test, $p = 0.004$) than the upper 30 cm, with a mean of 1.0 g $cm^{-3}$, ranging from 0.2 to 2.04 g $cm^{-3}$. The upper soil layer of 0 – 30 cm had a mean (± 1 S.D.) SOM density of 0.096 ± 0.035 g OM $cm^{-3}$ with values ranging from 0.021 to 0.21 g OM $cm^{-3}$. Soil core sections below the 0 – 30 cm interval had a mean SOM density of 0.095 ± 0.047 g OM $cm^{-3}$ with values ranging from 0.053 to 0.34 g OM $cm^{-3}$.

Our elemental analysis found that $SOM_{30}$ had a mean of 25% SOC (21 - 27%; 95% C.I.). Inorganic carbon accounted for an average of 2.5% (2.1 - 2.9%; 95% C.I.) of post-combusted soil dry mass (i.e., total carbon content of residues from LOI analysis). The percentage SOC values were later used for scaling predictions of $SOM_{30}$ to estimate total SOC stocks and uncertainties. No significant differences or correlations in OM density or C content existed between the 0-30, 40-60, and 70-90 cm sections of cores. Similar to the findings of Morris et al. (2016), we found a strong inverse relationship between LOI and bulk density.

3.2 Sub-pixel heterogeneity

A total of eighteen pixels contained multiple (2 or 3) soil core sites. SOM density varied by less than 0.025 g OM $cm^{-3}$ within fifteen of these pixels, however sub-pixel heterogeneity was over 0.05 g OM $cm^{-3}$ in three pixels (Fig 3). We examined field notes and aerial photos of these pixels to investigate potential explanations for higher and lower sub-pixel heterogeneity, which is reported in the Results section.

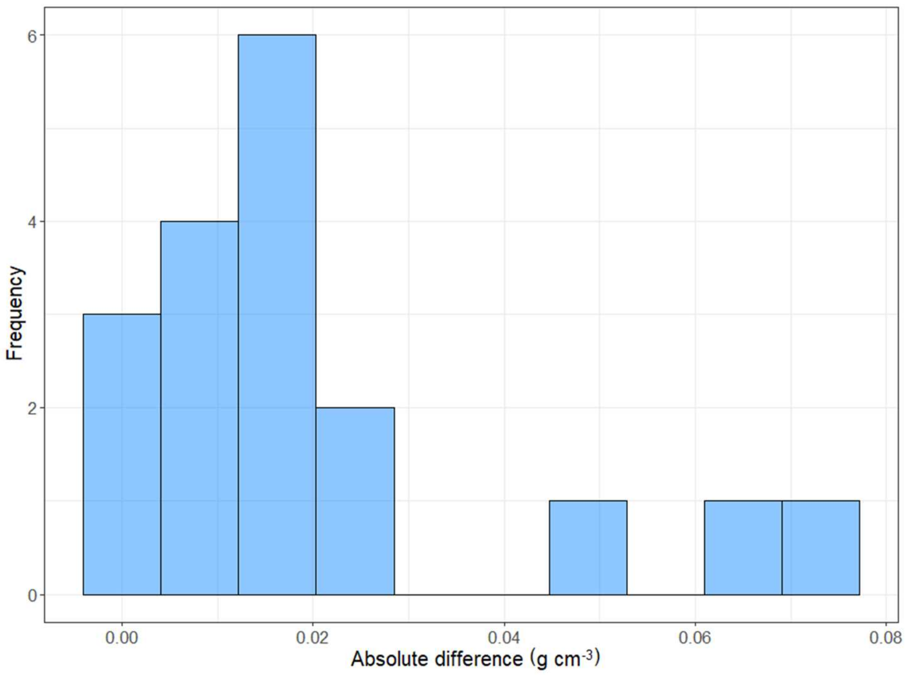

**Figure 3. Histogram of sub-pixel variability of $SOM_{30}$ expressed as the absolute difference between minimum and maximum of observations within a given Landsat-8 pixel.**

3.3 Model performance

The variable selection process yielded a set of three predictor statistics derived from the decade-long collection of Landsat-8 spectral indices. Final predictors were the mean value of NPV1 (NPV1.mean) and the standard deviations of NDVI (NDVI.sd) and MNDWI2 (MNDWI2.sd). These three predictors were used for model training and extrapolation of model predictions, while all other predictors were discarded.

The multiple linear regression fit to the training set had the formula:

$$\mathrm{SOM}_{30} = 3.40 * \mathrm{NPV1.mean} - 0.15 * \mathrm{NDVI.sd} + 2.48 * \mathrm{MNDWI2.sd} - 0.20 \quad [2]$$

The gradient boosted trees hyperparameter tuning process yielded a final model with 100 iterations, a learning rate of 0.03, gamma value of 0.9 (the minimum loss reduction necessary to continue splitting a regression tree), maximum tree depth of 2 (the number of potential splits in a regression tree), and subsample fraction of 0.5 (the fraction of randomly selected data for training a regression tree).

The gradient boosted trees model outperformed the multiple linear regression in all performance metrics, showing a strong predictive performance of $SOM_{30}$ on both the testing and training sets (Table 2; Fig 4).

**Table 2. Performance evaluation metrics for testing set (and training set) for the multiple linear regression and gradient boosted trees model.**

| Model | MAE (g OM cm$^{-3}$) | RMSE (g OM cm$^{-3}$) | $R^2$ |
|---|---|---|---|
| Multiple linear regression | 0.016 (0.020) | 0.022 (0.026) | 0.48 (0.47) |
| Gradient boosted trees | 0.012 (0.018) | 0.016 (0.023) | 0.67 (0.65) |

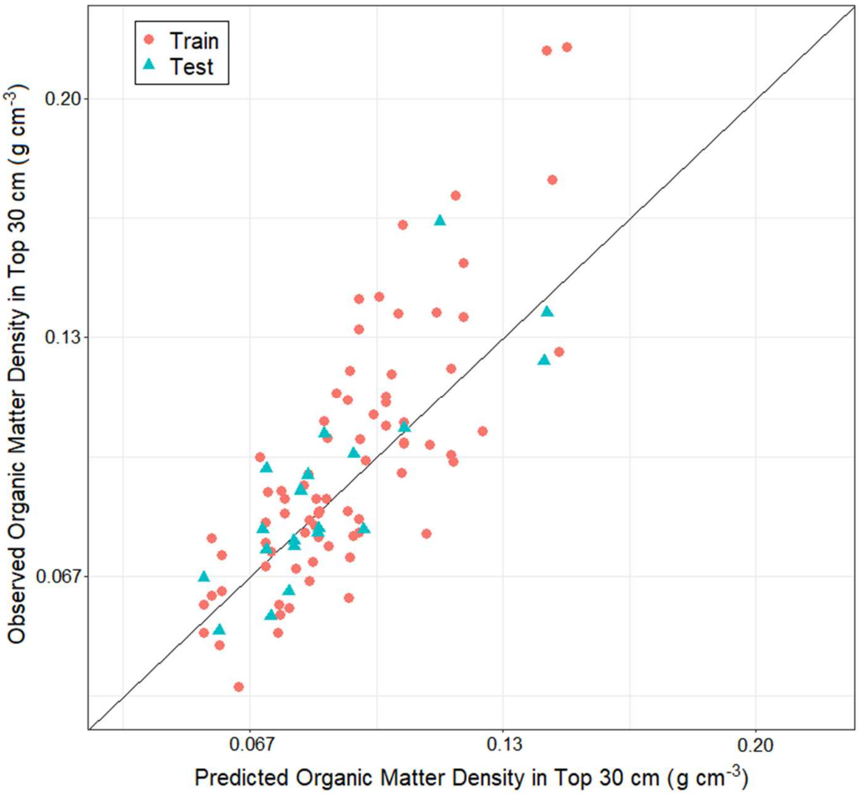


**Figure 4. Observed and model predicted (gradient boosted trees) $SOM_{30}$ for training (red circles) and testing (blue triangles) datasets. The black line represents an exact 1:1 equivalent.**

Despite its superior performance, the gradient boosted trees model has the drawback that it is more complicated to implement and less easy to interpret than a linear regression. However, there are still ways to assess its internal variable relationships. To investigate the relative influence of each predictor variable, we calculated Individual Conditional Expectations

(ICE) for each training data sample (Fig 5). ICE plots indicate how a prediction of a given instance (predicted SOM value in this case) will change over the range of each predictor variable within a complex machine learning model, allowing for some degree of interpretation of its individual variable dependencies. Seeing each instance allows the viewer to assess how consistent the response of a dependent variable is for a given predictor. If all instances show distinctly different responses, it may indicate complex variable relationships within the model. This is termed as the “marginal effect” of a predictor’s value on the model prediction. Overlaid on these plots is a smoothed general response across all training samples to illustrate the general effects of each predictor (Fig 5). We found that both NPV1.mean and MNDWI2.sd had generally positive effects on predicted $SOM_{30}$ similar to the coefficients in the linear regression (Eq. 2), while NDVI.sd effects varied substantially among samples (Fig 5). ICE curves were generated using the package “iml” in R (Interpretable Machine Learning; Molnar et al. 2018).

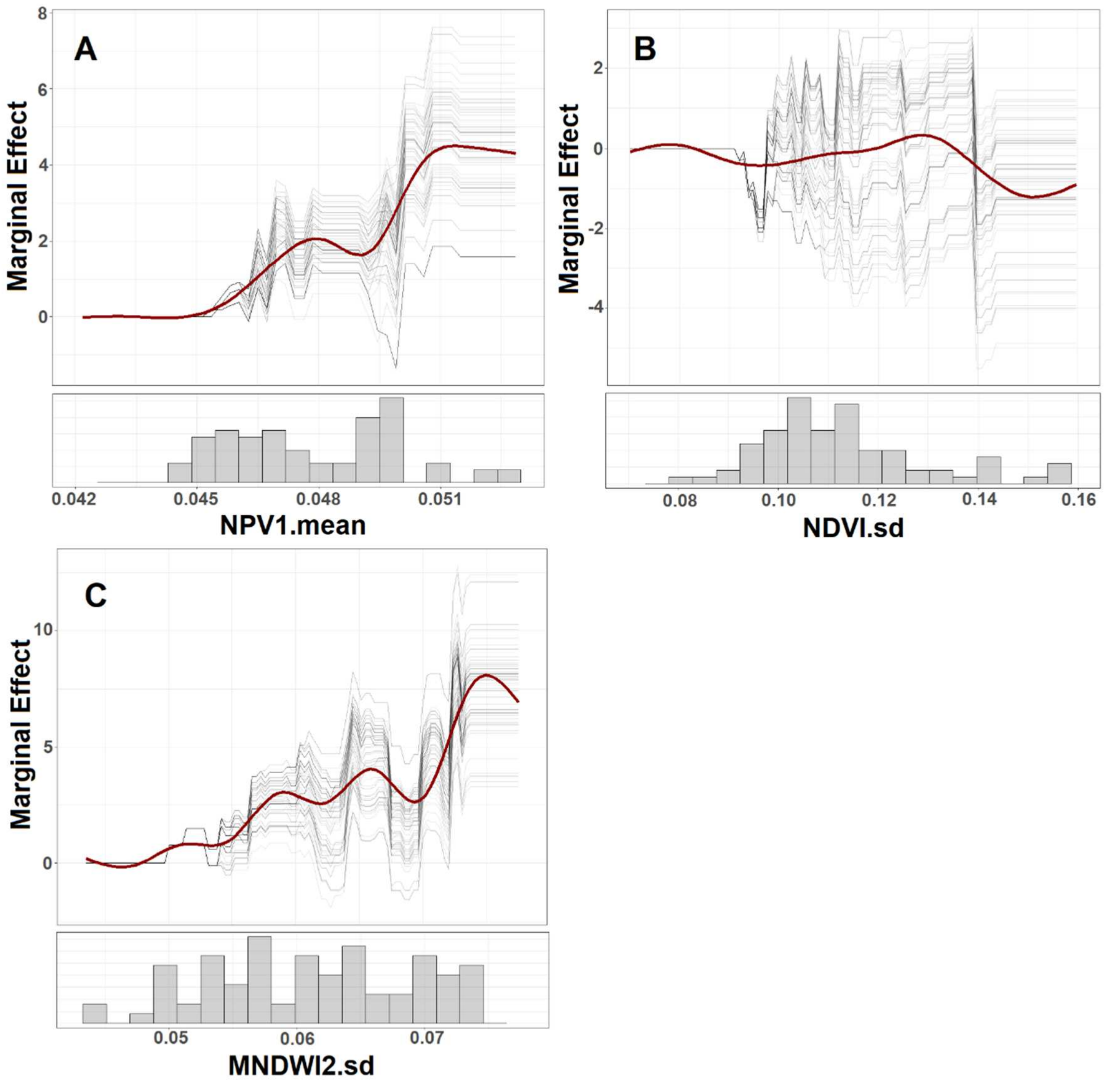


**Figure 5. Individual Conditional Expectation (ICE) curves plotted along with the general trend of marginal effects for each predictor variable on model predictions. Marginal histograms indicate the frequency distribution of predictors across the sample domain.**

3.4 Mapped OM density and total C stock estimation

Extrapolation of the gradient boosted trees model produced predicted spatial distributions of $SOM_{30}$ over a total of 14310 and 16550 Landsat-8 pixels for the Blackbird Creek and St. Jones River tidal marshes, respectively. These predictions were scaled to units of kg

OM $m^{-2}$ (within the upper 30 cm; Fig 6) and multiplied by the 30-by-30 m pixel area. This yielded a final estimate of 334.2 $\mp$ 68.8 Gg SOM (95% C.I.) and 438.0 $\mp$ 79.5 Gg SOM (95% C.I.) storage in the upper 30 cm of Blackbird Creek and St. Jones River tidal marshes, respectively. Using the estimated percentage of SOC in SOM from our LOI and elemental analysis, this equates to an estimated 76.9 (56.8 – 90.2) Gg OC and 100.7 (74.5 – 118.3) Gg OC storage in the upper 30 cm, respectively. Predicted $SOM_{30}$ tended to be greater in the high marsh of the central or lower reaches of the marsh systems and lesser in more inland and peripheral reaches (Fig 6). Predicted $SOM_{30}$ was generally lower in Blackbird Creek tidal marsh than in St. Jones River tidal marsh.

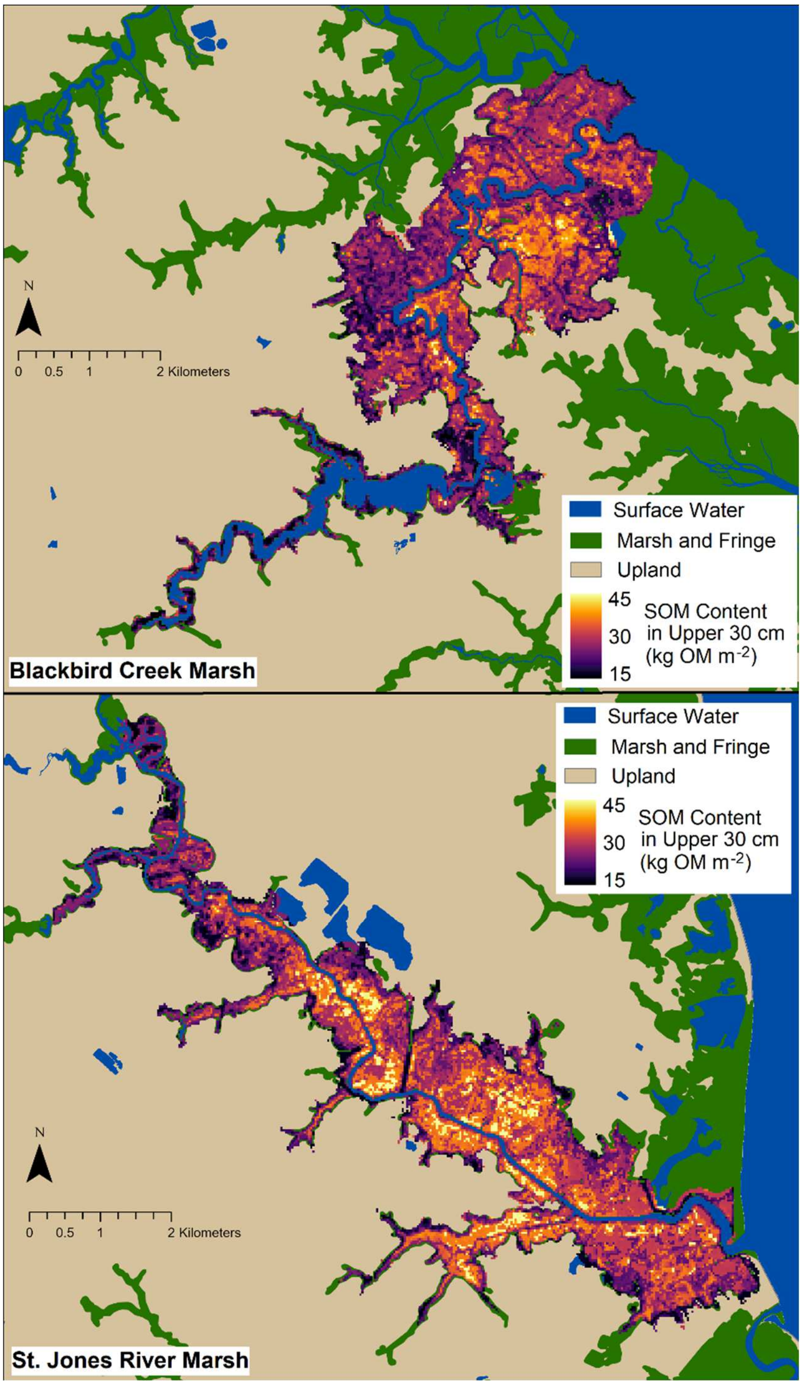


**Figure 6. Predicted spatial distributions of surficial soil organic matter (upper 30 cm) across the two study marshes. Warmer yellow and orange colors correspond to higher SOM density while darker tones correspond to lower densities.**

## 4. Discussion

### 4.1 Model predictors

The findings of this study demonstrated the potential of decadal spectral characteristics derived from the Landsat-8 OLI for modeling and mapping organic matter density in surficial tidal marsh soils. We found $SOM_{30}$ to vary spatially both within and across the two study marshes, indicating that some areas of the marshes store more SOM than others in their upper soil layers. This spatial heterogeneity was related to the average of a non-photosynthetic vegetation index and standard deviations of NDVI and a modified water index over the Landsat-8 record spanning from 2014-2023. The ICE plots in Figure 5 showed a positive marginal effect on predicted $SOM_{30}$ in pixels with high NPV1.mean and high MNDWI2.sd, which was also reflected in the positive coefficients of the multiple linear regression. The normalized difference between blue and green Landsat-8 bands (i.e., NPV1 in this study) has been identified as a predictor of aboveground biomass alongside other spectral indices (Byrd et al., 2018). MNDWI2 was developed to work in conjunction with NDVI as a spectral index for identifying small surface waterbodies and fine scale canal features (Reddy et al., 2018). Thus, the positive marginal effects of these predictors in our model suggest high $SOM_{30}$ in areas with abundant aboveground dead biomass and variable inundation status. The effects of NDVI.sd on model predictions were less clear, with some instances showing positive relationships and others negative (Fig 5). This would suggest that the variability of NDVI may have complex interactions with other predictors, and it may reflect the interactions of NDVI and MNDWI2 in identifying standing water on a landscape (Reddy et al., 2018). Maxwell et al. (2024) also found NDVI.sd to be a variable of moderate predictive importance for SOC density, but it is unclear what the variables effects were within that model. We note that while these predictors performed well in this study, their applicability may not be universal across all tidal salt marsh systems. Villoslada et al. (2022) found that the performance of different spectral predictors from aerial imagery varied across study sites and vegetation types, suggesting that some degree of local calibration may be necessary to maximize model performance in a given region of interest. This, along with the substantial landscape scale variation that this and other studies have observed, suggest that a single standardized approach for blue carbon inventorying with remotely sensed predictors would be less accurate, or inappropriate, when applied in a tidal salt marsh without local calibration.

The long period of record and high collection frequency of satellite missions like Landsat-8 allows for assessments of seasonal phenological and tidal inundation patterns. Such characteristics are not easily determined from data sources with infrequent collections, such as airborne LiDAR and aerial imagery programs like NAIP. However, these products are able to achieve much higher spatial resolution, and the fusion of such products with long-term satellite datasets may help overcome the limitations of any individual data source. For example, classification models of marsh fringe forests have recently demonstrated improved accuracy by incorporating airborne LiDAR information alongside multispectral aerial imagery (Powell et al., 2022). The results of this study reinforce the importance of ongoing and future remote sensing missions for blue carbon mapping and carbon cycle research at large. The upcoming Landsat Next mission will provide data products with higher spatial and spectral resolution, particularly in wavelengths relevant to NPV mapping (Dennison et al., 2023), and next-generation synthetic aperture radar could provide enhanced capabilities for deriving patterns of inundation and vegetation structural characteristics. These enhanced remote sensing products may improve blue carbon inventory accuracy and lead to better standardization of mapping techniques using publicly available satellite remote sensing data.

### 4.2 SOM and SOC characteristics and comparisons

Our observed percentage of SOC in SOM (25%) was lower than the average of 37% observed by (Wang et al., 2017) among salt marsh systems in Louisiana, USA, but fell within the broad range that they observed (12%-84%) and within the range observed previously in salt marshes in North Carolina, USA (22%-60%) (Craft et al., 1991). From the literature, it is clear this percentage can vary substantially across systems and soil textures. While we did not observe such large variability in percentages across the two study marshes, we note that local variability in the percentages of SOC in SOM could substantially influence estimates of salt marsh carbon stocks based on SOM measured with low-cost LOI analysis.

Scaling our mean observed surficial $SOM_{30}$ density to a volume of one cubic meter and multiplying by our estimated SOM:SOC ratio yielded an estimated SOC density (± 1 S.D.) of 24 ± 8.8 kg $m^{-3}$, which is only slightly lower the national mean value of 27 kg $m^{-3}$ proposed for coastal wetlands in the United States (Holmquist et al., 2018). At a per hectare scale, our estimates of SOC in the upper 30 cm were 60 (44 – 70) and 68 (50 – 79) Mg C $ha^{-1}$ for Blackbird Creek and St. Jones River tidal marshes, respectively. This was lower than a recent estimated global average of 83.1 Mg C $ha^{-1}$ (Maxwell et al., 2024), though well within its margin of uncertainty. This may suggest that the Blackbird Creek and St. Jones River coastal marshes may have a surficial SOC density typical of other salt marsh ecosystems in the USA and globally. However, comparing our whole marsh estimates of SOC in the top 30 cm to those of Wardrup et al. (2021), we estimated substantially lower SOC stored in both Blackbird Creek (this study: 77 Gg SOC, Wardrup et al.: 169 Gg SOC) and St. Jones River tidal marshes (this study: 101 Gg SOC, Wardrup et al.: 152 Gg SOC). The latter study utilized a regional scale model with training data from sites spanning the entirety of the northeastern United States. The discrepancy between these estimates may reflect the influence of local factors in our study marshes, such as the generally low SOC:SOM ratio we found in salt marsh soils. We note that local geology, vegetation, and geomorphology may all influence soil formation, and some degree of variability in SOM content across different systems is to be expected. These findings reinforce the importance of considering local characteristics in salt marsh SOM mapping, similar to the findings of Villoslada et al. (2022).

From our limited number of samples deeper than 30 cm, we found SOM content to be highly variable, with some samples exceeding the SOM content of the surface layer while others were much lower, which prevented us from projecting SOC estimates into deeper layers with much certainty. The total amount of SOC stored in these coastal marshes is certainly much higher than our estimates, but the thickness of marsh sediments (as well as its variability in space) is poorly understood in our study marshes. Some areas, such as the far upstream sites in St. Jones marsh had shallow sediment deposits with dense sand and gravel layers less than 30 cm from the surface, while most other areas extended deeper than our equipment was able to capture. Characterizing the depth of marsh sediment deposits is critical for accurately estimating the total amount of carbon and organic matter stored within coastal marshes (van Ardenne et al., 2018). This is no simple task, as sampling deep soils and measuring soil thickness requires larger, bulkier equipment that is logistically challenging to use in salt marsh systems and may require additional permits and regulatory review. The need for more observations and a fundamentally better understanding of deep salt marsh soil processes has been noted previously (Holmquist et al., 2018; Steinmuller & Chambers, 2019; van Ardenne et al., 2018; Wardrup, 2021), and we echo that here. This remains a major challenge in blue carbon accounting and a limitation for potential crediting systems.

### 4.3 Sub-pixel heterogeneity and limitations of scale

An obvious limitation of this study is the discrepancy between Landsat-8 pixel size (30 by 30 m) and the spatial coverage of individual soil cores. The long period of record and high collection frequency of satellite missions like Landsat-8 allows for assessments of seasonal phenological and tidal inundation patterns. Such characteristics are not easily determined from high resolution data sources with infrequent collections, such as airborne LiDAR and aerial imagery programs like NAIP. We found that $SOM_{30}$ varied little in most Landsat-8 pixels containing multiple soil coring locations (Fig 3). However, several pixels had large discrepancies in $SOM_{30}$ values, potentially due to heterogeneous vegetation patches and/or microtopography. The more heterogeneous pixels occupied areas of transitional marsh fringe vegetation or areas of “hummocky” marsh characteristics, where small tufts, or hummocks, of marsh grasses and sediments are interspersed with dense networks of drainage channels. Pixels with low sub-pixel SOM heterogeneity tended to be in the marsh interior with relatively homogenous vegetation and medium-to-high soil bulk densities. Future research that fuses high spatial, low temporal resolution products like aerial photographs, drone photogrammetry, and LiDAR with low spatial, high temporal resolution products like Landsat-8 may help resolve some of this sub-pixel spatial heterogeneity. For example, classification models of marsh fringe forests have recently demonstrated improved accuracy by incorporating airborne LiDAR information alongside multispectral aerial imagery (Powell et al., 2022). Future satellite remote sensing missions will also benefit blue carbon mapping efforts and carbon cycle research at large. The upcoming Landsat Next mission will provide data products with higher spatial and spectral resolution, particularly in wavelengths relevant to NPV mapping (Dennison et al., 2023), and next-generation synthetic aperture radar could provide enhanced capabilities for deriving patterns of inundation and vegetation structural characteristics. These enhanced remote sensing products may improve blue carbon inventory accuracy and lead to better standardization of mapping techniques using publicly available satellite remote sensing data.

Another limitation of this work is the “snapshot” nature of sample collection. All soil cores were collected in growing season months over the course of several years, which prevents assessments of potential seasonal and interannual variations in $SOM_{30}$. Previous studies have found that both salt marsh SOM concentrations and lateral OM export can vary on seasonal scales due to changes in salinity, inundation patterns, and vegetation phenology (Fettrow et al., 2023; Yuan et al., 2022; Zhao et al., 2016). Capturing a broad spatial assemblage of samples that also reflect seasonal or interannual variability would help enhance scientific understanding of blue carbon storage and accumulation rates in tidal salt marshes.

## 5. Conclusions

This study demonstrated the application of decadal statistics of satellite-derived spectral indices (in this case from the Landsat-8 OLI) for mapping surficial SOM stocks in tidal salt marshes. In just the to the top 30 cm of the marsh soil profile, we estimated that our two study marshes contain a combined 133-208 Gg SOC, the equivalent of roughly 490,000-760,000 metric tons of $CO_2$ if it were to be released to the atmosphere. Though this study was somewhat limited in sampling density and scope, we found substantial spatial heterogeneity of SOM within marsh systems in Delaware that may be driven by distributions of aboveground litter biomass (NPV1.mean), vegetation phenology (NDVI.sd), and tidal inundation patterns (MNDWI2.sd). However, we note that the performance of these predictors may vary in different systems. Our results indicate inconsistent levels of sub-pixel heterogeneity of SOM, which appear to be highest in fringe and hummocky marsh areas. Future research that fuses high resolution spatial datasets with multi-year satellite records may help resolve this, along with an increased *in situ* sampling density. Although we found no consistent spatial patterns in deeper soil layers in this specific study, we echo previous researchers in the need for greater accounting of deep SOM in blue carbon stock estimates. Larger and longer investigations may be facilitated through collaborations with National Estuarine Research Reserves and other established, on-site, coastal wetland management organizations. Improved methods for mapping landscape scale distributions of blue carbon and SOM will help guide targeted carbon inventorying and habitat protection efforts to minimize carbon loss due to human activities and sea level rise.

## 6. Acknowledgements

We would like to acknowledge our funding sources of the Delaware Department of Natural Resources and Environmental Control through the National Ocean and Atmospheric Administration award NA18NOS4200118. We acknowledge the Delaware National Estuarine Research Reserves, Kent County Department of Parks and Recreation, Delaware Department of Natural Resources and Environmental Control, and Delaware Wildlands groups for their permission for sampling access.

## 7. Data Availability

Grids of predicted surficial SOM from this study are available from the Environmental Data Initiative online data repository (https://portal.edirepository.org/nis/home.jsp).

Citation:

Warner, D.L. 2024. Predicted Surficial Blue Carbon Maps for Blackbird Creek and St. Jones River Tidal Salt Marshes using 2014-2023 Landsat-8 OLI records ver 1. Environmental Data Initiative. https://doi.org/10.6073/pasta/bd2271961d4f6b3701d5c3dfaaa48170

## 8. References

Andersen, T. J., Svinth, S., & Pejrup, M. (2011). Temporal variation of accumulation rates on a natural salt marsh in the 20th century - The impact of sea level rise and increased inundation frequency. *Marine Geology*, *279*(1–4), 178–187. https://doi.org/10.1016/j.margeo.2010.10.025

Araya-Lopez, R., de Paula Costa, M. D., Wartman, M., & Macreadie, P. I. (2023). Trends in the application of remote sensing in blue carbon science. *Ecology and Evolution*, *13*(9). https://doi.org/10.1002/ece3.10559

Baena, S., Moat, J., Whaley, O., & Boyd, D. S. (2017). Identifying species from the air: UAVs and the very high resolution challenge for plant conservation. *PLoS ONE*, *12*(11). https://doi.org/10.1371/journal.pone.0188714

Beaumont, N. J., Jones, L., Garbutt, A., Hansom, J. D., & Toberman, M. (2014). The value of carbon sequestration and storage in coastal habitats. *Estuarine, Coastal and Shelf Science*, *137*(1), 32–40. https://doi.org/10.1016/j.ecss.2013.11.022

Byrd, K. B., Ballanti, L., Thomas, N., Nguyen, D., Holmquist, J. R., Simard, M., & Windham-Myers, L. (2018). A remote sensing-based model of tidal marsh aboveground carbon stocks for the conterminous United States. *ISPRS Journal of Photogrammetry and Remote Sensing*, *139*, 255–271. https://doi.org/10.1016/j.isprsjprs.2018.03.019

Callahan, J.A., Horton, B.P., Nikitina, D.L., Sommerfield, C.K., McKenna, T.E., Swallow, D. (2017). Recommendation of Sea-Level Rise Planning Scenarios for Delaware. Technical Report prepared for Delaware Department of Natural Resources and Environmental Control (DNREC) Delaware Coastal Programs, p. 117. https://doi.org/10.13140/RG.2.2.17411.66082.

Chen, T., He, T., Benesty, M., Khotilovich, V., Tang, Y., Cho, H., Chen, K., Mitchell, R., Cano, I., Zhou, T., Li, M., Xie, J., Lin, M., Geng, Y., Li, Y., Yuan, J. (2024). xgboost: Extreme Gradient Boosting. R package version 1.7.7.1, https://CRAN.R-project.org/package=xgboost

Chmura, G. L., Anisfeld, S. C., Cahoon, D. R., & Lynch, J. C. (2003). Global carbon sequestration in tidal, saline wetland soils. *Global Biogeochemical Cycles*, *17*(4), n/a-n/a. https://doi.org/10.1029/2002gb001917

Chmura, G. L., Burdick, D. M., & Moore, G. E. (2012). Restoring salt marsh ecosystem services through tidal restoration. In C. T. Roman & D. M. Burdick (Eds.), *Tidal Marsh Restoration: A Synthesis of Science and Management* (pp. 233–251). Island Press.

Coxe, R. (2010). Delaware Statewide Vegetation Community Map. Delaware Department of Natural Resources and Environmental Control (DNREC), Division of Fish & Wildlife, Natural Heritage and Endangered Species Program.

Craft, C. B., Seneca, E. D., & Broome, S. W. (1991). Loss on ignition and kjeldahl digestion for estimating organic carbon and total nitrogen in estuarine marsh soils: Calibration with dry combustion. *Estuaries*, *14*(2), 175–179. https://doi.org/10.2307/1351691

Daughtry, C. S. T., Doraiswamy, P. C., Hunt, E. R., Stern, A. J., McMurtrey, J. E., & Prueger, J. H. (2006). Remote sensing of crop residue cover and soil tillage intensity. *Handbook of Environmental Chemistry, Volume 5: Water Pollution*, *91*(1–2), 101–108. https://doi.org/10.1016/j.still.2005.11.013

DeLaune, R. D., & White, J. R. (2012). Will coastal wetlands continue to sequester carbon in response to an increase in global sea level?: A case study of the rapidly subsiding Mississippi river deltaic plain. *Climatic Change*, *110*(1–2), 297–314. https://doi.org/10.1007/s10584-011-0089-6

Dennison, P. E., Lamb, B. T., Campbell, M. J., Kokaly, R. F., Hively, W. D., Vermote, E., Dabney, P., Serbin, G., Quemada, M., Daughtry, C. S. T., Masek, J., & Wu, Z. (2023). Modeling global indices for estimating non-photosynthetic vegetation cover. *Remote Sensing of Environment*, *295*. https://doi.org/10.1016/j.rse.2023.113715

DNERR. (1999). Delaware National Estuarine Research Reserve: Estuarine Profile. Prepared by the Delaware Department of Natural Resources and Environmental Control.

Fagherazzi, S., Kirwan, M. L., Mudd, S. M., Guntenspergen, G. R., Temmerman, S., D'Alpaos, A., Van De Koppel, J., Rybczyk, J. M., Reyes, E., Craft, C., & Clough, J. (2012). Numerical models of salt marsh evolution: Ecological, geomorphic, and climatic factors. *Reviews of Geophysics*, *50*(1), 1–28. https://doi.org/10.1029/2011RG000359

Fettrow, S., Wozniak, A., Michael, H. A., & Seyfferth, A. L. (2023). Factors controlling spatiotemporal variability of soil carbon accumulation and stock estimates in a tidal salt marsh. In *EGUsphere* (Issue December).

Heiri, O., Lotter, A. F., & Lemcke, G. (2001). Loss on ignition as a method for estimating organic and carbonate content in sediments: reproducibility and comparability of results. *Journal of Paleolimnology*, *25*(1), 101–110. https://doi.org/https://doi.org/10.1023/A:1008119611481

Holmquist, J. R., Windham-Myers, L., Bliss, N., Crooks, S., Morris, J. T., Megonigal, J. P., Troxler, T., Weller, D., Callaway, J., Drexler, J., Ferner, M. C., Gonneea, M. E., Kroeger, K. D., Schile-Beers, L., Woo, I., Buffington, K., Breithaupt, J., Boyd, B. M., Brown, L. N., … Woodrey, M. (2018). Accuracy and Precision of Tidal Wetland Soil Carbon Mapping in the Conterminous United States. *Scientific Reports*, *8*(1), 9478. https://doi.org/10.1038/s41598-018-26948-7

Kirwan, M. L., & Megonigal, J. P. (2013). Tidal wetland stability in the face of human impacts and sea-level rise. *Nature*, *504*(7478), 53–60. https://doi.org/10.1038/nature12856

Kuhn, M. (2008). Building Predictive Models in R Using the caret Package. Journal of Statistical Software, 28(5), 1–26. doi:10.18637/jss.v028.i05

Maxwell, T. L., Spalding, M. D., Friess, D. A., Murray, N. J., Rogers, K., Rova, A. S., Smart, L. S., Weilguny, L., Adame, M. F., Adams, J. B., Copertino, M. S., Cott, G. M., de Paula Costa, M. D., Holmquist, J. R., Ladd, C. J. T., Lovelock, C. E., Ludwig, M., Moritsch, M. M., Navarro, A., … Worthington, T. A. (2024). Soil carbon in the world's tidal marshes (Pre-print). 1–30. https://doi.org/10.1101/2024.04.26.590902

McBratney, A. B., Mendonça Santos, M. L., & Minasny, B. (2003). On digital soil mapping. *Geoderma*, 117(1–2). https://doi.org/10.1016/S0016-7061(03)00223-4

McFeeters, S.K. (1996). The use of the Normalized Difference Water Index (NDWI) in the delineation of open water features. International Journal of Remote Sensing, 17(7). 1425-1432. 10.1080/01431169608948714

McLeod, E., Chmura, G. L., Bouillon, S., Salm, R., Björk, M., Duarte, C. M., Lovelock, C. E., Schlesinger, W. H., & Silliman, B. R. (2011). A blueprint for blue carbon: Toward an improved understanding of the role of vegetated coastal habitats in sequestering CO2. *Frontiers in Ecology and the Environment*, *9*(10), 552–560. https://doi.org/10.1890/110004

Molnar C., Bischl B., Casalicchio G. (2018). iml: An R package for Interpretable Machine Learning. Journal of Open Source Software, 3(26), 786. doi:10.21105/joss.00786

Montero, D., Aybar, C., Mahecha, M. D., Martinuzzi, F., Söchting, M., & Wieneke, S. (2023). A standardized catalogue of spectral indices to advance the use of remote sensing in Earth system research. *Scientific Data*, *10*(1), 1–20. https://doi.org/10.1038/s41597-023-02096-0

Morris, J. T., Barber, D. C., Callaway, J. C., Chambers, R., Hagen, S. C., Hopkinson, C. S., Johnson, B. J., Megonigal, P., Neubauer, S. C., Troxler, T., & Wigand, C. (2016). Contributions of organic and inorganic matter to sediment volume and accretion in tidal wetlands at steady state. *Earth's Future*, *4*(4), 110–121. https://doi.org/10.1002/2015EF000334

Mueller, P., Do, H. T., Jensen, K., & Nolte, S. (2019). Origin of organic carbon in the topsoil of Wadden Sea salt marshes. *Marine Ecology Progress Series*, *624*, 39–50. https://doi.org/10.3354/meps13009

Ocean Policy Committee. (2023). *Ocean Climate Action Plan* (Vol. 77).

Oreska, M. P. J., McGlathery, K. J., Aoki, L. R., Berger, A. C., Berg, P., & Mullins, L. (2020). The greenhouse gas offset potential from seagrass restoration. *Scientific Reports*, *10*(1), 1–15. https://doi.org/10.1038/s41598-020-64094-1

Pham, T. D., Ha, N. T., Saintilan, N., Skidmore, A., Phan, D. C., Le, N. N., Viet, H. L., Takeuchi, W., & Friess, D. A. (2023). Advances in Earth observation and machine learning for quantifying blue carbon. *Earth-Science Reviews*, *243*(May 2022), 104501. https://doi.org/10.1016/j.earscirev.2023.104501

Powell, E. B., Laurent, K. A. S., & Dubayah, R. (2022). Lidar-Imagery Fusion Reveals Rapid Coastal Forest Loss in Delaware Bay Consistent with Marsh Migration. *Remote Sensing*, *14*(18). https://doi.org/10.3390/rs14184577

R Core Team (2024). R: A Language and Environment for Statistical Computing. R Foundation for Statistical Computing, Vienna, Austria. <https://www.R-project.org/>.

Reddy, S. L. K., Rao, C. V., Kumar, P. R., Anjaneyulu, R. V. G., & Krishna, B. G. (2018). A novel method for water and water canal extraction from Landsat-8 OLI imagery. *The International Archives of the Photogrammetry, Remote Sensing and Spatial Information Sciences*, *XLII–5*(5), 323–328. https://doi.org/10.5194/isprs-archives-XLII-5-323-2018

Rouse, J.W., Haas, R.H., Scheel, J.A., and Deering, D.W. (1974). Monitoring Vegetation Systems in the Great Plains with ERTS. Proceedings, 3rd Earth Resource Technology Satellite (ERTS) Symposium, vol. 1, p. 48-62. https://ntrs.nasa.gov/citations/19740022614

Sharma, R., Mishra, D. R., Levi, M. R., & Sutter, L. A. (2022). Remote Sensing of Surface and Subsurface Soil Organic Carbon in Tidal Wetlands: A Review and Ideas for Future Research. *Remote Sensing*, *14*(12), 1–21. https://doi.org/10.3390/rs14122940

St. Laurent, K. A., Hribar, D. J., Carlson, A. J., Crawford, C. M., & Siok, D. (2020). Assessing coastal carbon variability in two Delaware tidal marshes. *Journal of Coastal Conservation*, *24*(6), 1–16. https://doi.org/10.1007/s11852-020-00783-3

Steinmuller, H. E., & Chambers, L. G. (2019). Characterization of coastal wetland soil organic matter: Implications for wetland submergence. *Science of the Total Environment*, *677*, 648–659. https://doi.org/10.1016/j.scitotenv.2019.04.405

Sweet, W. V., Hamlington, B. D., Kopp, R. E., Weaver, C. P., Barnard, P. L., Bekaert, D., Brooks, W., Craghan, M., Dusek, G., Frederikse, T., Garner, G. G., Gens, A. S., Krasting, J. P., Larour, E., Marcy, D., Marra, J. J., Obeysekera, J., Osler, M., Pendleton, M., … Zuzak, C. (2022). Global and Regional Sea Level Rise Scenarios for the United States. In *NOAA Technical Report NOS CO-OPS 083* (Issue February).

Theuerkauf, E. J., Stephens, J. D., Ridge, J. T., Fodrie, F. J., & Rodriguez, A. B. (2015). Carbon export from fringing saltmarsh shoreline erosion overwhelms carbon storage across a critical width threshold. *Estuarine, Coastal and Shelf Science*, *164*, 367–378. https://doi.org/10.1016/j.ecss.2015.08.001

Torio, D. D., & Chmura, G. L. (2013). Assessing Coastal Squeeze of Tidal Wetlands. *Journal of Coastal Research*, *290*(5), 1049–1061. https://doi.org/10.2112/jcoastres-d-12-00162.1

Uhran, B., Windham-Myers, L., Bliss, N., Nahlik, A. M., Sundquist, E. T., & Stagg, C. L. (2021). Improved Wetland Soil Organic Carbon Stocks of the Conterminous U.S. Through Data Harmonization. *Frontiers in Soil Science*, *1*(October), 1–16. https://doi.org/10.3389/fsoil.2021.706701

van Ardenne, L. B., Jolicouer, S., Bérubé, D., Burdick, D., & Chmura, G. L. (2018). The importance of geomorphic context for estimating the carbon stock of salt marshes. *Geoderma*, *330*(June), 264–275. https://doi.org/10.1016/j.geoderma.2018.06.003

Villoslada, M., Sipelgas, L., Bergamo, T. F., Ward, R. D., Reintam, E., Astover, A., Kumpula, T., & Sepp, K. (2022). Multi-source remote sensing data reveals complex topsoil organic carbon dynamics in coastal wetlands. *Ecological Indicators*, *143*(July), 109329. https://doi.org/10.1016/j.ecolind.2022.109329

Wang, H., Piazza, S. C., Sharp, L. A., Stagg, C. L., Couvillion, B. R., Steyer, G. D., & McGinnis, T. E. (2017). Determining the Spatial Variability of Wetland Soil Bulk Density, Organic Matter, and the Conversion Factor between Organic Matter and Organic Carbon across Coastal Louisiana, U.S.A. *Journal of Coastal Research*, *33*(3), 507–517. https://doi.org/10.2112/JCOASTRES-D-16-00014.1

Wardrup, J. L. (2021). Soil organic carbon in tidal wetlands of the northeast United States. University of Delaware, Department of Plant and Soil Sciences.

Wardrup, J., Guevara, M., Llamas, R., Correll, M.D., Hantson, W., Shriver, G., Vasilas, B., & Vargas, R. (2021). Soil Organic Carbon Distributions in Tidal Wetlands of the Northeastern USA. ORNL DAAC, Oak Ridge, Tennessee, USA. https://doi.org/10.3334/ORNLDAAC/1905

Witte, S., & Giani, L. (2017). Genesis of soils from Holocene tidal deposits at the North Sea coast. *Catena*, *156*(July 2016), 124–130. https://doi.org/10.1016/j.catena.2017.04.006

Yuan, Y., Li, X., Xie, Z., Xue, L., Yang, B., Zhao, W., & Craft, C. B. (2022). Annual Lateral Organic Carbon Exchange Between Salt Marsh and Adjacent Water: A Case Study of East Headland Marshes at the Yangtze Estuary. *Frontiers in Marine Science*, *8*(January), 1–15. https://doi.org/10.3389/fmars.2021.809618

Zhang, C., Mishra, D. R., & Pennings, S. C. (2019). Mapping salt marsh soil properties using imaging spectroscopy. *ISPRS Journal of Photogrammetry and Remote Sensing*, *148*(January), 221–234. https://doi.org/10.1016/j.isprsjprs.2019.01.006

Zhao, Q., Bai, J., Liu, Q., Lu, Q., Gao, Z., & Wang, J. (2016). Spatial and Seasonal Variations of

Soil Carbon and Nitrogen Content and Stock in a Tidal Salt Marsh with Tamarix chinensis, China. *Wetlands*, *36*, 145–152. https://doi.org/10.1007/s13157-015-0647-1